Equilibrium Optimizer Tuned Frequency-shifted Internal Model Control Proportional-Derivative Decoupled Dual-loop Design for Industrial Plants followed by Experimental Validation

Pulakraj Aryan[a], *G. Lloyds Raja[b] and Ramon Vilanova[c]

[a]Center for Sustainable Energy, Indian Institute of Technology, Roorkee- 247667, Uttarakhand, India;

[b]Electrical Engineering Department, National Institute of Technology Patna, Ashok Rajpath, Patna-800005, Bihar, India;

[c]Department of Telecommunications and Systems Engineering, Autonomous University of Barcelona, Spain

(Correspondence: lloyds.ee@nitp.ac.in, lloyd.raja@gmail.com)

Equilibrium Optimizer Tuned Frequency-shifted Internal Model Control Proportional-Derivative Decoupled Dual-loop Design for Industrial Plants followed by Experimental Validation

Abstract

Integrating and unstable processes require rugged control demand by virtue of their non-self-regulation character. The occurrence of system poles located at the origin and on the right half of the complex frequency plane causes instability in an open-loop configuration. When these processes proceed with dead time, it demands more sophisticated control requirements. Therefore, binal-loop control schemes are recommended over single-loop controller schemes. For plants with prevalent unstable and integrating dynamics and dead time, a novel modified inferred internal model control- proportional derivative decoupled binal-loop control system is suggested. The inner-loop is controlled by the stabilizing proportional derivative controller with Routh-Hurwitz stability constraints. The outer-loop contains an inferred internal model controller for reference-point tracking. The equilibrium optimizer is then used to minimize the integral squared error by tuning the inner and outer-loop controller settings in the confined search space. The suggested strategy delivers appreciable enhancement in the quantitative performance measures as compared to some of the contemporary control techniques. The effect of time-varying disturbance and robust stability analysis is also presented. Finally, utilizing a magnetic levitation laboratory setup, the suggested method is experimentally verified using the hardware-in-loop method.

Keywords

Binal-loop control, inferred internal model control, integrating and unstable, dead-time, integral squared error, constrained equilibrium optimizer.

Nomenclature

List of symbols

M_S- Maximum sensitivity
ψ- Robustness parameter
L- Loop transfer function
R- Reference signal (set-point)
D- Disturbance signal
U- Control effort
G_P- Process model
$\hat{G}_P$- Frequency-shifted model ($G_P(s-\psi)$)
Y- Plant output
Gc_1- Outer-loop controller
Gc_2- Inner loop controller
θ- Time delay of the process
τ- Time constant of the process
K_C- Proportional gain
τ_D- Derivative gain
ρ- Control measure volume

m- mass lying in ρ
V- Volumetric surge
K_e- Equilibrium concentration
R_p- Proliferation rate
R_t- Turnover rate
δ- Iteration index
χ- Present iteration
χ_m- Maximum iteration
T_s- Settling time
PO_s- Peak overshoot
PU_s- Peak undershoot

Abbreviations

IMC: Internal Model Control
MI^{2}MC: Modified Inferred IMC
DS: Direct Synthesis
B-DoF: Binal Degree of Freedom
RH: Routh-Hurwitz
PSO: Particle Swarm Optimization
ITAE: Integral Time Absolute Error
ITSE: Integral Time Squared Error
ISE: Integral Squared Error
IAE: Integral Absolute Error
IPTD: Integrating Plus Time Delay
UFOPTD: Unstable First-order Plus Time Delay
SOIPTD: Second Order Integrating Plus Time Delay
USOPTD: Unstable Second Order Plus Time Delay
PID: Proportional Integral Derivative
PID-P: Proportional Integral Derivative Proportional (dual loop)
DL-SP: Dual Loop with Smith Predictor
PD-PID: Proportional-Derivative Proportional-Integral-Derivative (dual loop)
PI-PD: Proportional-Integral Proportional-Derivative (dual loop)
I-PD: Integral Proportional-Derivative (dual loop)
FOIMC: Fractional Order IMC
RIMC: Relocated IMC
EO: Equilibrium Optimizer

1 | INTRODUCTION

1.1 Unstable and integrating plants: an outline

Plants with unstable open-loop poles are frequently observed especially in chemical industries. The operations of reactors, polymerisers, heat exchangers and distillators exhibit unstable dynamics [1]. On the other hand, the enactments of batch processes such as silo tanks, pump storage, distillation units and other liquid-level systems exhibit integrating dynamics. These processes empirically have origin pole(s) in the complex frequency plane. The integrating

processes are unable to self-regulate in the event of the introduction of any disturbance signal which results in uncontrollable process output. The other issue with these (unstable and integrating) processes is the inherent presence of time delay. The delay can arise due to mechanical lags such as transportation or velocity and also due to the existence of utility loops such as composition analyzers and recyclers [2]. These delays account for the supplementary phase lag which leads to the destabilization of the plant in a closed-loop environment and thereby posing a stringent control requirement. When it comes to the control schemes for unstable and integrating processes, the volume of the available literature is significantly lesser than that for the control of stable systems (having stable open-loop poles) [3]. A summary of control methods for the unstable and integrating types of processes is presented in Table 1.

1.2 Controllers in a unity feedback configuration

Unity feedback configuration due to its unsophistication and compliance is a favored strategy for designing controllers. PID controllers are often used for single-loop designs. Sree and Chidambaram [4] used an unstable filter coupled with a PI controller to regulate unstable bioreactors. PID controllers are commonly designed using direct synthesis (DS) [5, 6], target characteristic equation fitting [7], maximum sensitivity-based design [8], error function reduction [9], and internal model control (IMC) oriented designing [10-12]. Designing PID with the IMC approach is a prominent mechanism as it requires lesser tunable requirements. Other PID design methodologies employed by researchers include the scaled loss of performance method [13] and H_2 minimizing [14].

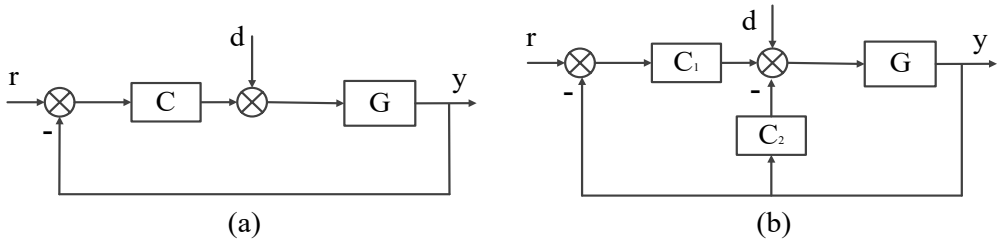

Figure 1. Controller schemes (a) Unity-feedback (b) Binal-loop

1.3 Binal-loop control configuration

Binal or two-loop configuration is better equipped in meeting control requirements of the unstable and integrating natured process [15-18]. With the exception of an extra inner-loop intended to stabilize the plant before to being subjected to outer-loop control, the structure of the binal-loop is akin to that of a unity feedback scheme. Figure 1 reveals the structures of unity feedback and binal-loop configuration.

Park et al. [19] were amongst the initial researchers who came up with the binal-loop controller design for handling unstable processes. The binal-loop method of [20] used the IMC technique for PID in the outer-loop to go with the proportional (P) inner-loop controller tuned using the Ziegler-Nichols method. In [21], a Smith predictor was used with a binal-loop for handling unstable plants. Smith predictor acts as the dead-time compensator for dominant time-delayed processes. [22] reported a binal-degree of freedom (B-Dof) control method which was an enhancement of the parallel control architecture [23]. PI-PD has turned out to be a popular binal-loop scheme in recent times with several researchers showing interest in it [18,24-28]. As the name suggests, PID is replaced with PI in the outer-loop while PD is adopted in the

inner-loop for stabilization purposes. In the PI-PD structure proposed by [24], the controllers were fashioned incorporating the model predictive control technique. [25-27] obtained a convex stabilization region to find the settings of PI-PD controller graphically. Routh-Hurwitz (RH) criteria and moment matching technique was utilized by [18] to design their PI-PD scheme. By removing the P gain from the outer-loop controller of the PI-PD scheme, it is further modified to I-PD structure. Few researchers have utilized this structure for processes with integrating dynamics [29,30].

Table 1. A brief summary of integrating and unstable process control methods

Author	Controller configuration	Design method	Nature of process	No. of tuning parameters	Remarks
Rao and Chidambaram [2]	PI/PID with unstable filter	DS	Integrating and unstable	Five	Unity feedback
Sree and Chidambram [4]	PI	DS	Unstable	Three	Unity feedback
Rao et al. [5]	PID with lead-lag	DS	Integrating	Five	Unity feedback
Vanavil et al. [6]	PID with lead-lag	DS	Unstable	Five	Unity feedback
Chanti Babu et al. [7]	PID	Desired characteristic equation	Unstable	Four	Unity feedback
Panda [10]	PID	DS	Integrating and unstable	Five	Unity feedback
Vanavil et al. [11]	IMC incorporated PID with lead-lag	H_2 optimal closed-loop transfer function	Integrating and unstable	Four	Unity feedback
Verma and Padhy [12]	Indirect IMC incorporated PID	Maximum sensitivity and closed-loop stability	Stable	Four	Unity feedback
Ali and Majhi [9]	PID	ISE minimization	Integrating	Three	Unity feedback
Arrieta et al. [13]	PID	Weighted performance degradation	Integrating and unstable	Four	Unity feedback
Ghosiya Begam et al. [14]	IMC based PID	H_2 minimization	Non-minimum phase integrating	Four	Unity feedback
Park et al. [19]	PID-P	RH stability	Unstable	Four	Binal-loop
Vijayan and Panda [20]	IMC based PID-P	Ziegler Nichols	Stable and unstable	Four	Binal-loop
Cong et al. [21]	DL-SP	Characteristic equation stabilization	Unstable	Four	Binal-loop
Ajmeri and Ali [22]	B-DoF	DS	Unstable	Five	2 degree of freedom
Ajmeri and Ali [23]	PD-PID	DS	Integrating	Five	Parallel control
HongboZou and Li [24]	PI-PD	Model predictive control	Unstable	Four	Binal-loop
Raja and Ali [18]	PI-PD	RH stability and moment resembling	Integrating and unstable	Four	Binal-loop

Onat [25]	PI-PD	Centroid of the convex stability region	Unstable	Four	Binal-loop
Nema and Padhy [35]	PI-PD	Cuckoo optimizer	Unstable	Four	Binal-loop
Irshad and Ali [28]	PI-PD	PSO	Integrating	Four	Binal-loop
Kaya [34]	PI-PD	PSO	Integrating	Four	Binal-loop
Alyoussef and Kaya [26]	PI-PD	Analytical centroid based geometrical	Integrating and unstable	Four	Binal-loop
Alyoussef and Kaya [27]	PI-PD	Analytical centroid based geometrical	Integrating	Four	Binal-loop
Chakraborty et al. [29]	I-PD	Gain margin, phase margin	Integrating	Four	Binal-loop
Kaya and Peker [30]	I-PD	minimizing time moment weighted integrated performance measures	Integrating	Three	Binal-loop
Kumari et al. [8]	FOIMC-PD/P	RH stability and Maximum sensitivity	Unstable	Four	Binal-loop
Kumari et al. [1]	FOIMC-PID	Coefficient matching	Unstable	Five	Binal-loop
Kumar et al. [36]	FOIMC-PD	ITSE minimization	Double integrating	Five	Decoupled binal-loop
Aryan et al. [15]	RIMC-PD	EO	Integrating and unstable	Four	Binal-loop
Aryan et al. [16]	RIMC-PD	EO	Inverse response integrating and unstable	Four	Binal-loop

1.4 Overview of Optimization

There are mainly two ways of solving optimization problems: (1) deterministic and (2) stochastic. In the deterministic approach, the problems are formulated into linear and non-linear programming. In [31], the authors have introduced the application of linear programming for process control. These methods involve the gradient approach to find the solution in the search space. Problems are numerically optimized by formulating certain objective functions. The mathematical models developed are uniform and have no randomness [32]. Though effective, they suffer the drawback of returning the local optima when subjected to nonlinear and non-convex-natured real-world contentions. Stochastic methods on the other hand which include meta-heuristic algorithms, produce and utilize random variables [33]. They are independent of the nature of the problem and, in contrast to deterministic approaches, do not require mathematical intricacies of the problem. These methods are becoming popular due to their flexibility which makes allowance for solving any type of optimization problem without tinkering with the algorithm's structure. The capacity to break out of local optima using characteristics for exploration and exploitation is another crucial factor. Due to these merits, stochastic tuning methods are getting a lot of attention. Few researchers have also utilized this approach in binal-loop controllers. Particularly, Irshad and Ali [28] and Kaya [34] have used particle swarm optimization (PSO) to tune their PI-PD controller while Nema and Padhy [35] have achieved it by the cuckoo optimizer. Equilibrium optimizer (EO) [33] has emerged as a

prominent tool in various process control applications [36]. Recently, Douger [37] have used EO for tuning a Smith predictor based I-PD controller. The selection of an objective function is vital when using the metaheuristic approach. These include ISE [28,17], integral time absolute error (ITAE) [38] and integral squared time cubed error [34].

1.5 Key research gaps and Motivation

1. Aryan et al. [15] was the first literature to extend the pole-shifting principle of Verma and Padhy [12] for unstable and integrating plants by augmenting the same with RH stability criteria and EO. This approach was extended for inverse response processes in [16]. However, both proposals in [15] and [16] have three main drawbacks:

- A non-decoupled binal-loop control structure was used and hence the changes in stabilizing controller design/settings impact the outer-loop controller settings.
- The stabilizing PD controller assumes a fixed derivative gain which is half of the delay value irrespective of the plant model.
- An arbitrary search range is used for the robustness parameter.

2. In recent decoupled/non-decoupled binal-loop/B-DoF strategies for controlling unstable/integrating processes [23,38,22], the selectable controller parameters were determined by means of comprehensive simulation research. A superior substitute for the controller design employed in the aforementioned works is an optimal controller design with the explicit goal of enhancing performance metrics.

3. One of the drawbacks of optimal controller design lies in its aggressive control efforts and poor robustness while improving requisite performance measures [35,28]. Such aggressive control efforts can be reduced by imposing certain constraints while finding optimal settings so as to ensure robustness.

4. EO has achieved massive recognition in recent times. However, it is yet to be applied to a decoupled control strategy for process control applications.

1.6 Present work and Contributions

The modified inferred IMC-PD (MI^2MC-PD) scheme aims to combine the advantages of decoupled control loops, inferred IMC (pole-shifting) principle which is a robust control technique, effective PD design and the constrained equilibrium optimizer such that a satisfactory performance/robustness tradeoff is achieved. To obtain the constrained search space for the inner-loop PD controller, RH stability criteria are used. This search space is finally utilized by the modified constrained EO algorithm to attain the optimal equilibrium point (controller settings) corresponding to minimal ISE. The efficacy of the recommended scheme is tested through extensive simulation studies and comparing quantitative performance measures. The robustness of the suggested scheme is established through the assessment of performance measures on the perturbed plant model and robust stability tests. The MI^2MC-PD scheme overcomes the drawbacks of [15] as discussed in the motivation section as follows:

1. As the outer-loop is decoupled from the inner in the present work, the controllers have an independent set of equations that allows the stabilizing controller to be adjusted without affecting the servo response. This flexibility helps the control structure to deal with

disturbances which can occur at any instant during the course of plant operation without adjusting the outer-loop controller settings [39].
2. Though Pade approximation [40] is used to get a constrained search space, the optimal PD settings are selected from the search space using equilibrium optimizer instead of fixing the derivative gain to be half of the process dead time.
3. The range of robustness parameter is selected such that the relation between the parameter and maximum sensitivity is linear.

The highlights of this work are conveyed below:

- Redesigning indirect IMC into a MI^{2}MC-PD decoupled binal loop structure suitable for delayed unstable/integrating plants.
- Finding RH criteria-based constrained search-space followed by ISE minimization with EO for designing PD controller.
- Outer-loop optimal controller settings are obtained using EO with M_S considerations thus ensuring that robustness is not sacrificed in search of optima.
- The practical feasibility of the MI^{2}MC-PD scheme is investigated through an experimental verification utilizing a magnetic levitation setup.

2 | THEORETICAL BACKGROUND

The stability margins of a closed-loop system are directly impacted by the pole and zero shift. The indirect design approach (IDM) is based on this. According to Verma and Padhy's report on IDM [12], the following assertions are made:

2.1 Proposition-1: If the loop transfer function for any stable process $L_1(s)= C(s)G(s)$ and frequency-shifted process $L_2(s)=C(s)G(s-\psi)$ have maximum sensitivities Ms_1, Ms_2 and phase margins φg_1, φg_2 respectively, the following relationships are satisfied: (1) $Ms_1 \leq Ms_2$ and $\varphi g_1 \geq \varphi g_2 \; \forall \; \psi \geq 0$ (2) $Ms_1 > Ms_2$ and $\varphi g_1 < \varphi g_2 \; \forall \; \psi < 0$.

2.2 Proposition-2: Consider that controllers $C_1(s)$, $C_2(s)$ are used for processes $G(s-\psi)$, $G(s)$ respectively. Then, the maximum sensitivities Ms_1, Ms_2 corresponding to loop transfer functions $L_1(s)=C_1(s)G(s)$ and $L_2(s)=C_2(s)G(s)$ satisfy the following inequalities: (1) $Ms_1 \leq Ms_2$ $\forall \; \psi \geq 0$ (2) $Ms_1 > Ms_2 \; \forall \; \psi < 0$.

Hence, 'ψ' determines the robustness while designing controllers. It can be understood from proposition-2 that if a controller is fashioned for $G(s-\psi)$ rather than $G(s)$, then in such a case the robustness of the system can be instituted on the choice of ψ. The proof of the above propositions can be found in [12]. A typical second-order delayed process can be represented as

$$G_P(s) = \frac{Ke^{-\theta s}}{a_2 s^2 + a_1 s + a_0} \tag{1}$$

where, K/a_0 ($a_0 \neq 0$) is the gain and θ is the delay. Coefficients a_2, a_1 and a_0 are used to determine the type of processes as follows:

i) IPTD for $a_2=a_0=0$, $a_1=1$
ii) UFOPTD for $a_0<0$, $a_1>0$, $a_2=0$
iii) SOIPTD for $a_0=0$, a_2, $a_1>0$
iv) USOPTD for a_2, $a_1>0$, $a_0=-1$

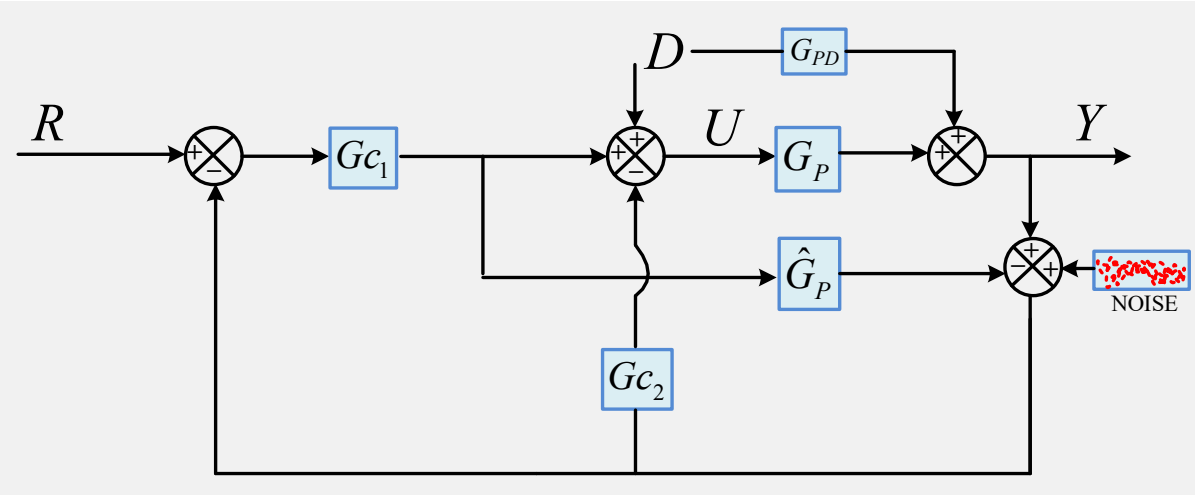

Figure 2. The decoupled binal-loop control structure

3 | CONTROL SCHEME

The recommended design comprises two controllers, one in each loop. Gc_1 is the outer-loop MI^{2}MC controller responsible for reference tracking, while the PD controller Gc_2 stabilizes the inner-loop and is also responsible for rejecting the effect of disturbances. Figure 2 reveals the suggested decoupled binal-loop control scheme. RH criteria provide the range of operational settings for Gc_2 parameters which are discussed in the sections ahead. This range is finally used by the EO algorithm to get the optimal settings by minimizing the quadratic performance index ISE which is given as

$$ISE = \int_0^t e^2(t)dt,\ e(t) = R(t) - Y(t) \tag{2}$$

3.1 Decoupling

The closed-loop transfer function for set-point tracking is given by

$$\frac{Y}{R} = \frac{Gc_1G_P}{1 + Gc_1G_P - Gc_1\hat{G}_P + Gc_2G_P - Gc_2\hat{G}_P} \tag{3}$$

As ψ is small, $\hat{G}_P \approx G_P$ (3) reduces to

$$\frac{Y}{R} \approx Gc_1G_P \tag{4}$$

Similarly, the inner-loop transfer function for disturbance rejection is given by

$$\frac{Y}{D} = \frac{(1 - Gc_1\hat{G}_P)G_P}{1 + Gc_2G_P + Gc_1G_P - Gc_1\hat{G}_P} \tag{5}$$

As ψ is small, $\hat{G}_P \approx G_P$ (5) reduces to

$$\frac{Y}{D} \approx \frac{(1 - Gc_1\hat{G}_P)G_P}{1 + Gc_2G_P} \tag{6}$$

The expression of the servo transfer function given in (4) is independent of Gc_2. This implies that the servo controller can be tuned independently without affecting the regulatory response. Similarly, the characteristic equation of regulatory response given in (6) is free from servo controller Gc_1. Hence, the suggested binal-loop scheme exhibits decoupling considering the

fact that ψ is small. This is further established with the dynamic response of a test example $G_P(s) = 0.2e^{-s}/s(4s+1)$ given in Figure 3. In this test example, the servo response is attained by applying a unit step signal 'R' at t=0s while to analyze the regulatory behavior, a disturbance D=-1 is subjected at t=50s. The change of Gc_2 parameters do not affect the servo response vindicating the decoupling effect as evident from Figure 3.

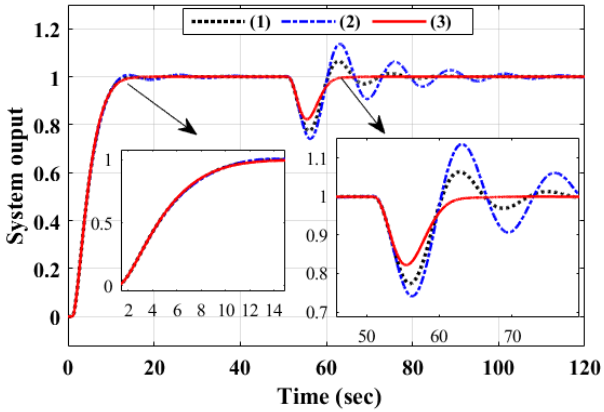

Figure 3. Dynamic response of test example under varying regulatory control: (1)- *Gc_2=1(1+s)*, (2)- *Gc_2=1.5(1+1.5s)*, (3)- *Gc_2=2(1+2s)*

3.2 Inner-loop

Gc_2 is the stabilizing PD controller expressed by the following equation:

$$Gc_2 = K_C(1 + \tau_D s) \tag{7}$$

To comment on inner-loop stability, the characteristic equation of (6) needs to be analyzed which is given as follows:

$$1 + Gc_2 G_P = 0 \tag{8}$$

Equation (8) is subjected to RH stability analysis for various plant models in the following subsections:

3.2.1 First-order processes (IPTD and UFOPTD). Consider an IPTD process given by

$$G_P = \frac{Ke^{-\theta s}}{s} \tag{9}$$

Substituting (7) and (9) in (8), the characteristic equation is obtained as

$$1 + \frac{KK_C(1 + \tau_D s) \times e^{-\theta s}}{s} = 0 \tag{10}$$

For controller design purposes, Pade's first-order approximation of the delay term in the characteristic equation is a prevalent method. Applying Pade's first-order approximation [40] $e^{-\theta s} \approx \frac{(1-0.5\theta s)}{(1+0.5\theta s)}$, (10) can be modified as

$$s + KK_C(1 + \tau_D s)\left(\frac{1 - 0.5\theta s}{1 + 0.5\theta s}\right) = 0 \tag{11}$$

After re-arranging the terms, (11) becomes

$$(0.5\theta - 0.5\theta KK_C\tau_D)s^2 + (1 - 0.5\theta KK_C + KK_C\tau_D)s + KK_C = 0 \tag{12}$$

Applying RH stability criteria on (12), the following inequalities can be obtained:

$$\left.\begin{array}{c} KK_C > 0 \\ KK_C < \dfrac{1}{\tau_D} \\ KK_C < \dfrac{1}{(0.5\theta - \tau_D)} \end{array}\right\} \tag{13}$$

Similarly, for the UFOPTD process given in (14), the constraints for the inner-loop are obtained as given in (15).

$$G_P = \frac{Ke^{-\theta s}}{\tau s - 1} \tag{14}$$

$$\left.\begin{array}{c} KK_C > 1 \\ KK_C < \dfrac{1}{\tau_D} \\ KK_C < \dfrac{(0.5\theta - \tau)}{(0.5\theta - \tau_D)} \end{array}\right\} \tag{15}$$

3.2.2 Second-order processes (SOIPTD and USOPTD). Consider a SOIPTD process given by

$$G_P = \frac{Ke^{-\theta s}}{s(\tau s + 1)} \tag{16}$$

Substituting (7) and (16) in (8), the characteristic equation is obtained as

$$1 + \frac{KK_C(1 + \tau_D s) \times e^{-\theta s}}{s(\tau s + 1)} = 0 \tag{17}$$

Once again utilizing Pade's approximation $e^{-\theta s} \approx \frac{(1-0.5\theta s)}{(1+0.5\theta s)}$, (17) can be modified as

$$s(\tau s + 1) + KK_C(1 + \tau_D s)\left(\frac{1 - 0.5\theta s}{1 + 0.5\theta s}\right) = 0 \tag{18}$$

After arranging the terms, (18) can be rewritten as

$$0.5\theta\tau s^3 + (0.5\theta + \tau - 0.5\theta KK_C\tau_D)s^2 + (1 + KK_C(\tau_D - 0.5\theta))s + KK_C = 0 \tag{19}$$

Applying RH stability criteria on (19), the following inequalities can be obtained:

$$\left.\begin{array}{c} KK_C > 0 \\ KK_C < \dfrac{0.5\theta + \tau}{(0.5\theta\tau_D)} \\ (0.5\theta\tau_D(0.5\theta - \tau_D)(KK_C)^2 - 0.5\theta(0.5\theta + \tau)KK_C + 0.5\theta + \tau) > 0 \end{array}\right\} \tag{20}$$

Along similar lines, for a USOPTD process given as in (21), the constraints for the inner-loop are obtained as given in (22).

$$G_P = \frac{Ke^{-\theta s}}{(\tau_1 s - 1)(\tau_2 s + 1)} \tag{21}$$

$$\left.\begin{array}{c} KK_C > 0 \\ KK_C < \dfrac{\tau_1 - \tau_2 + \tau_1\tau_2}{\tau_D} \\ ((\tau_1 - \tau_2 + \tau_1\tau_2 - KK_C\tau_D) \times (\tau_1 - \tau_2 + 0.5\theta + KK_C(\tau_D - 0.5\theta)) - \tau_1\tau_2(1 + KK_C)) > 0 \end{array}\right\} \quad (22)$$

where, $\tau_1 > \tau_2$. A summary of stabilizing constraints discussed in the previous section is presented in Table 2.

Table 2. Constraints on Gc_2

1st Order Process	Constraints on K_C and τ_D	2nd Order Process	Constraints on K_C and τ_D
IPTD	$KK_C > 0$ $KK_C < \dfrac{1}{\tau_D}$ $KK_C < \dfrac{1}{(0.5\theta - \tau_D)}$	**SOIPTD**	$KK_C > 0$ $KK_C < \dfrac{0.5\theta + \tau}{(0.5\theta\tau_D)}$ $\begin{pmatrix} 0.5\theta\tau_D(0.5\theta - \tau_D)(^K \\ -0.5\theta(0.5\theta + \tau)KK_C + 0.5\theta + \tau \end{pmatrix} > 0$
UFOPTD	$KK_C > 1$ $KK_C < \dfrac{1}{\tau_D}$ $KK_C < \dfrac{(0.5\theta - \tau)}{(0.5\theta - \tau_D)}$	**USOPTD**	$KK_C > 0$ $KK_C < \dfrac{\tau_1 - \tau_2 + \tau_1\tau_2}{\tau_D}$ $\begin{pmatrix} (\tau_1 - \tau_2 + \tau_1\tau_2 - KK_C\tau_D) \times \\ (\tau_1 - \tau_2 + 0.5\theta + KK_C(\tau_D - 0.5\theta)) \\ -\tau_1\tau_2(1 + KK_C) \end{pmatrix} > 0$

3.3 Outer-loop

Following proposition-2 which explains the effect of pole shifting on robustness [41], the Gc_1 for tracking R is designed for the augmented model $G_P(s - \psi)$ instead of $G_P(s)$. For the processes discussed in equation (1), the augmented model is given as

$$G_P(s - \psi) = \hat{G}_P(s) = \frac{\hat{K}e^{-\theta s}}{\hat{a}_2 s^2 + \hat{a}_1 s + \hat{a}_0} \quad (23)$$

where, $\hat{K} = Ke^{\varphi\theta}$, $\hat{a}_2 = a_2$, $\hat{a}_1 = (a_1 - 2\varphi a_2)$ and $\hat{a}_0 = (a_2\varphi^2 - a_1\varphi + a_0)$. $\hat{G}_P(s)$ is decomposed as

$$\hat{G}_P(s) = \hat{G}_P^-(s) \times \hat{G}_P^+(s) \quad (24)$$

In (24), $\hat{G}_P^-(s)$and $\hat{G}_P^+(s)$ corresponds to the invertible and non-invertible constituents of $\hat{G}_P(s)$ respectively. Now, the MI^{2}MC controller Gc_1 is given by

$$Gc_1(s) = \left[\hat{G}_P^-(s)\right]^{-1} H_f(s) \quad (25)$$

$H_f(s)$ stands for a low-pass filter. The generic expression of Gc_1 is given by

$$Gc_1(s) = \left(\frac{\hat{a}_2 s^2 + \hat{a}_1 s + \hat{a}_0}{\hat{K}}\right) \times \frac{1}{(\lambda s + 1)^n} \quad (26)$$

n is the order of $H_f(s)$ which relies on $\hat{G}_P(s)$ and λ is a tunable parameter. A summary of Gc_1 for different plants is given in Table 3.

Table 3. Structure of Gc_1 for different processes

Process	Filter ($H_f(s)$)	MI²MC controller (Gc_1)
IPTD	$\frac{1}{\lambda s+1}$	$\left(\frac{s}{\hat{K}}\right)\times\frac{1}{(\lambda s+1)}$
UFOPTD	$\frac{1}{\lambda s+1}$	$\left(\frac{\hat{\tau}s-1}{\hat{K}}\right)\times\frac{1}{(\lambda s+1)}$
SOIPTD	$\frac{1}{\lambda s^2+2\lambda s+1}$	$\left(\frac{s(\hat{\tau}s+1)}{\hat{K}}\right)\times\frac{1}{(\lambda s^2+2\lambda s+1)}$
USOPTD	$\frac{1}{\lambda s^2+2\lambda s+1}$	$\left(\frac{(\hat{\tau}_1 s-1)(\hat{\tau}_2 s+1)}{\hat{K}}\right)\times\frac{1}{(\lambda s^2+2\lambda s+1)}$

3.4 Selection of ψ

The selection of robustness parameter ψ is an important aspect of the proposed controller design [12, 41]. The criteria of minimal ISE selection cannot be utilized in this regard because The default value of ψ =0 results in minimum ISE. Proposition 2 explains how the regulated system's robustness is jeopardized at this level. Furthermore, the performance metric degrades significantly with large values of ψ. Therefore, while choosing the value of ψ, a proper tradeoff needs to be made. The authors of [12] looked on how ψ affected the stable process. An IPTD process's loop transfer function (LTF), $e^{-0.5s}/s$, has been examined here using a similar methodology (Figure 4). As seen in Figure 4(a), the frequency plot moves to the origin in the complex plane as ψ moves from negative to positive values. Conversely, as previously said, the divergence of output y from the setpoint (unity) falls with ψ (minimum for ψ = 0) in the time domain response plot (Figure 4(b)) for the positive value of ψ. To further strengthen this claim, the variation of ψ with M_S is studied to verify the applicability of proposition 2.

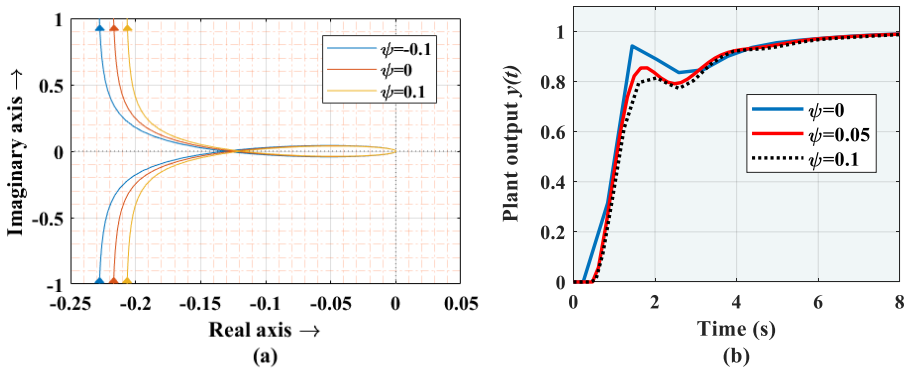

Figure 4. Impact of ψ: (a) Nyquist plot of the LTF $G_{C1}(s)\,G_P(s-\psi)$ (b) Closed-loop response of $G_P(s-\psi)$

4 | CONSTRAINED EQUILIBRIUM OPTIMIZER ALGORITHM

EO is a member of the metaheuristic algorithm family. The scientific ideas guiding the equilibrium state of inert substances serve as its source of inspiration [33]. It repeats the mass conservation concept as constituents transfer by skipping into or out of the search space

volume. In this algorithm, the concentration indicates the place, and the particle stands for the solution. These particles' ultimate goal is to locate the equilibrium state that best represents the solution. This transition is described by the first-order mass balancing equation as follows:

$$\rho \frac{dm}{dt} = VK_e - Vm + R_p \tag{27}$$

where ρ is the controlling volume and m is the mass contained therein.

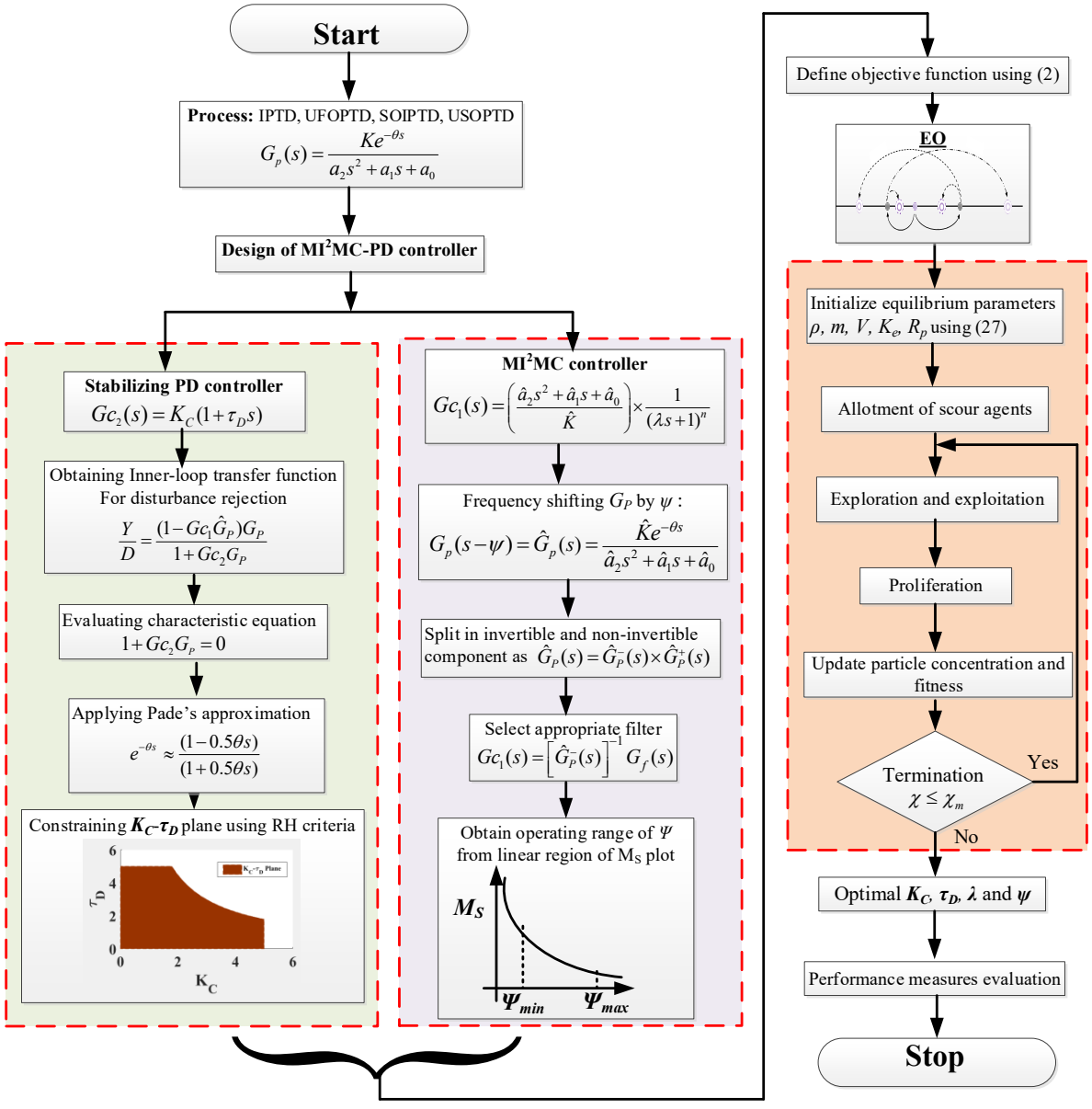

Figure 5. Proposed constrained EO flowchart with controller design framework

The rate at which mass changes inside ρ is given by $\rho\, dm/dt$. V is the volumetric surge rate of entering and leaving ρ. R_p is the proliferation rate, while K_e is the equilibrium concentration. ρ, V, R_p and K_e as mentioned in (27) are the components of mass balancing equation from which EO algorithm mimics its operation. The initial values of these parameters are taken from [33] as ρ=1, V=rand (0,1), R_p= 0.5 and K_e= zeros (1, dim). Here, 'rand (0,1)' stands for any number randomly initialized in the range (0,1) and zeros (1, dim) creates a null vector of size '1 x specified dimension'. In constrained EO, the particles are given a reduced search space to find the optimal location.

This enhances the algorithm's efficacy for faster convergence and improved fitness. This is achieved by making following changes to the algorithm:

- Utilizing the inequalities given in equations (13), (15), (20) and (22), the constraints on the K_C-τ_D plane are calculated by running a simple subroutine.
- This search leeway is provided to the EO algorithm for obtaining ρ.

The algorithm is then proceeded by steps that include initialization, allotment of scour agents, exploration, exploitation, proliferation and termination to provide the optimal solution. The details of these steps can be found in [33] and Aryan et al. [15]. A brief flowchart with controller design framework is depicted in Figure 5.

5 | SIMULATION RESULTS AND DISCUSSION

After constraining the search space, EO finds the equilibrium point at minimal ISE as discussed in the previous section. This approach was tested on an IPTD process $e^{-0.5s}/s$ and compared with other algorithms for the optimal location. In Figure 6(a) y-axis indicates 'fitness'. Smaller the fitness value, the better the performance of the algorithm. Thus Figure 6(a) justifies the selection of EO in the present proposal. It was noticed that EO illustrated better convergence characteristics than the other algorithms at the end of 20 iterations (refer to Figure 6(a)). After 20 iterations, the fitness value was almost constant. The metaheuristic techniques do not give unique solutions since they are based on iterative methods [33,15-17]. The solutions obtained after multiple independent runs are slightly different from each other though each solution is unique and representative of the optima of a particular run [42]. It is best practice to select the optimal settings after repeated runs rather than a single run [33]. Table 4 presents the statistical data of those independent runs. As shown in Figures 6(b) and 6(c), the quadratic performance measure ISE offers a respectable trade-off between various time-domain measurements due to its capacity to reduce oscillations and big amplitude in the dynamic response of process output. The recommended control strategy is tested for its suitability to commonly encountered integrated and unstable industrial process models after EO and ISE have been chosen. These benchmark process models ranging from first-order to fifth-order are widely used in literature [6,15,17,18,20,22,23,27-30,43-47]. A plot of ψ vs M_S for these examples is presented in Figure 7. M_S is found to be an approximately linear function of ψ when it is limited between -0.05 and 0.05. However, only positive values of ψ are considered ([0, 0.05] for all examples) to be consistent with Proposition-2. The suggested scheme is compared with the methods adopted by afore-cited works in terms of dynamic time-domain measures such as settling time (T_s), the magnitude of peak overshoot (PO_s) and peak undershoot (PU_s) along with the comparison of integral performance measures (ISE and IAE). These measures are analyzed for reference tracking (servo) and disturbance rejection (regulatory) abilities separately. The M_S values of outer and inner loops are calculated separately to vindicate the robustness of the MI^{2}MC-PD scheme. Since it is impossible to model any industrial process exactly, various levels of perturbation are considered in plant models. Controller settings as derived for the unperturbed model were used to simulate the dynamic responses of the perturbed models to further illustrate the robustness of the MI^{2}MC-PD scheme. The servo and regulatory responses are attained by applying a positive 'R' unit step and a negative 'D' step signal (refer to Figure 2). In practice, setpoint changes and disturbances can occur at any time when the plant is in operation. So, the controller must ensure that the Y follows reference R by rejecting disturbance D from time to time. Hence, both R and D are applied (as drive signals) during optimization such that the closed-loop response (involving both servo and regulatory action) is taken into consideration

while evaluating the objective function. As equilibrium optimizer has the ability to simultaneously search multiple search spaces for an optimal point, it has been exploited in this work to achieve optimal closed-loop response (involving both servo and regulatory action). Though it is possible to tune both controllers separately, it will add to the computation time. Hence, it is worth tuning both controllers simultaneously having established the fact that both loops are decoupled.

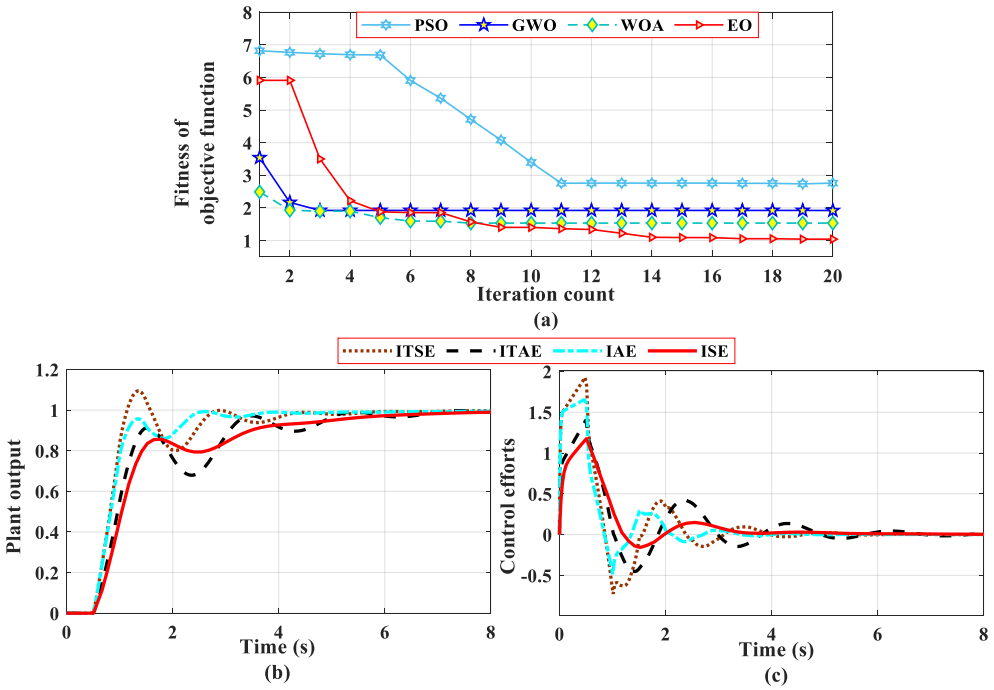

Figure 6. Response to unit step set point for the process $e^{-0.5s}/s$ (a) convergence curves for different optimization methods (*PSO: Particle swarm optimization, GWO: Grey wolf optimization, WOA: Whale optimization*) (b) plant output for various fitness functions (c) control efforts for various fitness functions

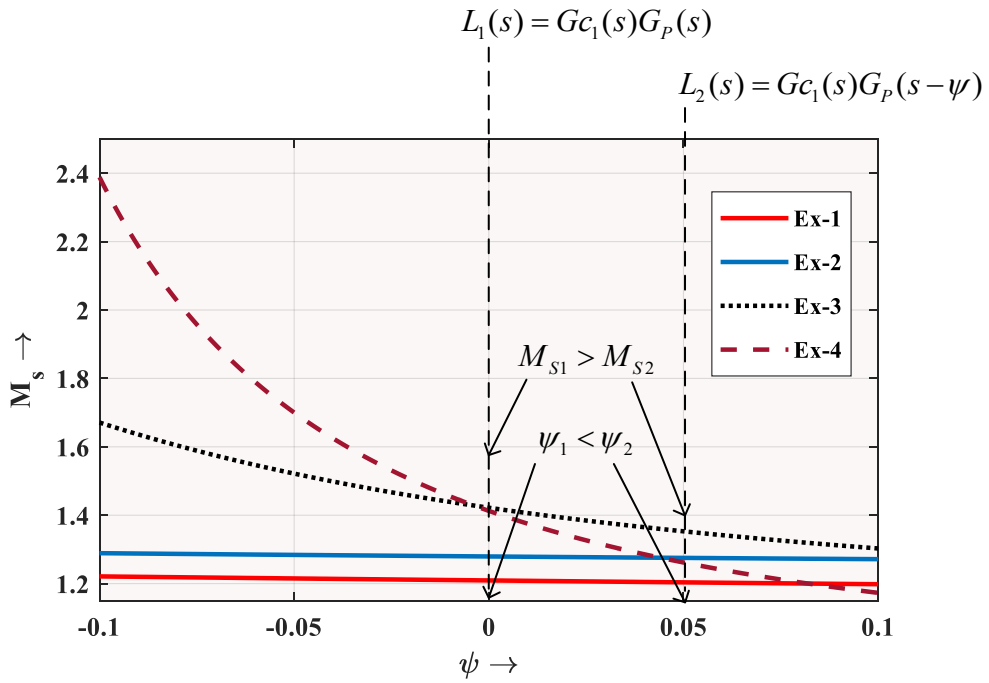

Figure 7. The plot of ψ vs Ms for all examples

Table 4. Statistical data of independent runs

ISE_{MAX}	ISE_{MIN}	ISE_{AVE}	ISE_{STD}	Run Time
1.814346607	0.9959019628	1.255023	0.3629765	264.90 s

5.1 First-order examples

One example each from IPTD and UFOPTD categories is considered. The performance measures for both nominal as well as perturbed cases are computed. Constrained K_C-τ_D search-space for optimal equilibrium location obtained from (13) and (15) are shown in Figure 8. The final optimal settings from constrained EO are given in Table 5. Table 6 and Table 7 present the performance measure comparison under nominal and different levels of perturbed conditions respectively. It must be noted that for unity feedback methods having a single controller, only one M_S value (i.e. outer) is tabulated, while for binal-loop schemes, both inner and outer loop ($M_{S1}$and M_{S2}) are calculated separately to ensure fairness in comparison.

5.1.1 Example 1 (IPTD). In Ajmeri and Ali [23], the following controller parameters are used for $G_P(s) = e^{-0.5s}/s$: K_{c1} = 1.4967, T_{d1} = 0.2377, λ=0.3281, τ=0.6026, K_{c2} = 1.6604, T_{i2} = 2.0576 and T_{d2} = 0.1771. The above controller settings were designed at M_S=2. For the same process, the respective PID controllers with filters suggested in [43] and [44] are: $G_c = 1.4361\left(1+1/2.312s+0.223s\right)\left(1/0.1369s+1\right)$ and $G_c = 1.3436\left(1+0.25495s\right)\left(1+1.1364s/1+0.025495s\right)$. To assess the regulatory behavior, D = -1 is applied at t=15 sec. Achieved closed-loop 'Y' with 'U' is given in Figure 9(a) and Figure 9(b). The design methods of [23], [43] and [44] give remarkably large POs for the servo (Y/R) response. Though the T_s of the recommended scheme is slightly higher, it delivers much lesser PU_s than other discussed methods during the regulatory (Y/D) action. The 'U' amplitude during the set-point tracking is also significantly greater for compared works which is undesirable. From Figure 9, it is evident that the MI^{2}MC-PD scheme provides relatively uniform 'U', better Y/R and Y/D which is also reflected in the performance measures in Table 6. Particularly for servo, the IAE and ISE measure of the MI^{2}MC-PD scheme is 1.58 and 0.952 respectively which is much lesser than the counterparts. The M_S values of the suggested method for inner and outer loops (M_{S1}=1.205 and M_{S2}=1.358) are also appreciably lower than other methods (refer to Table 6).

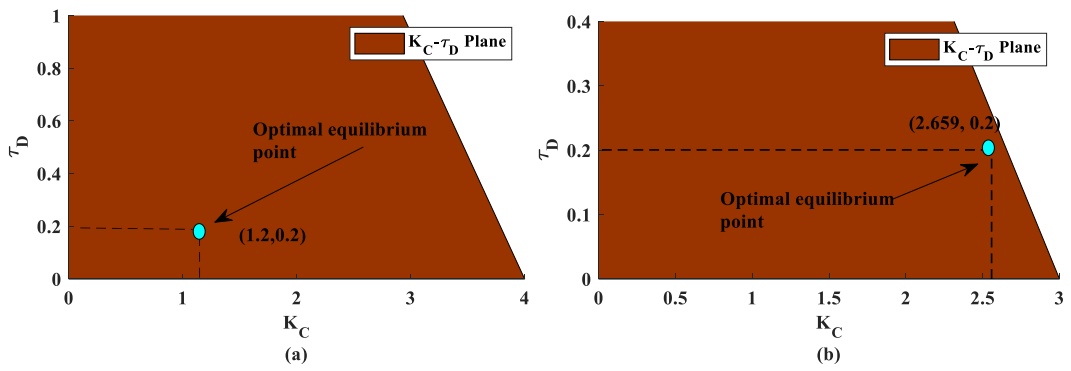

Figure 8. Constrained search-space with optimal equilibrium location (a) Example-1 (b) Example-2

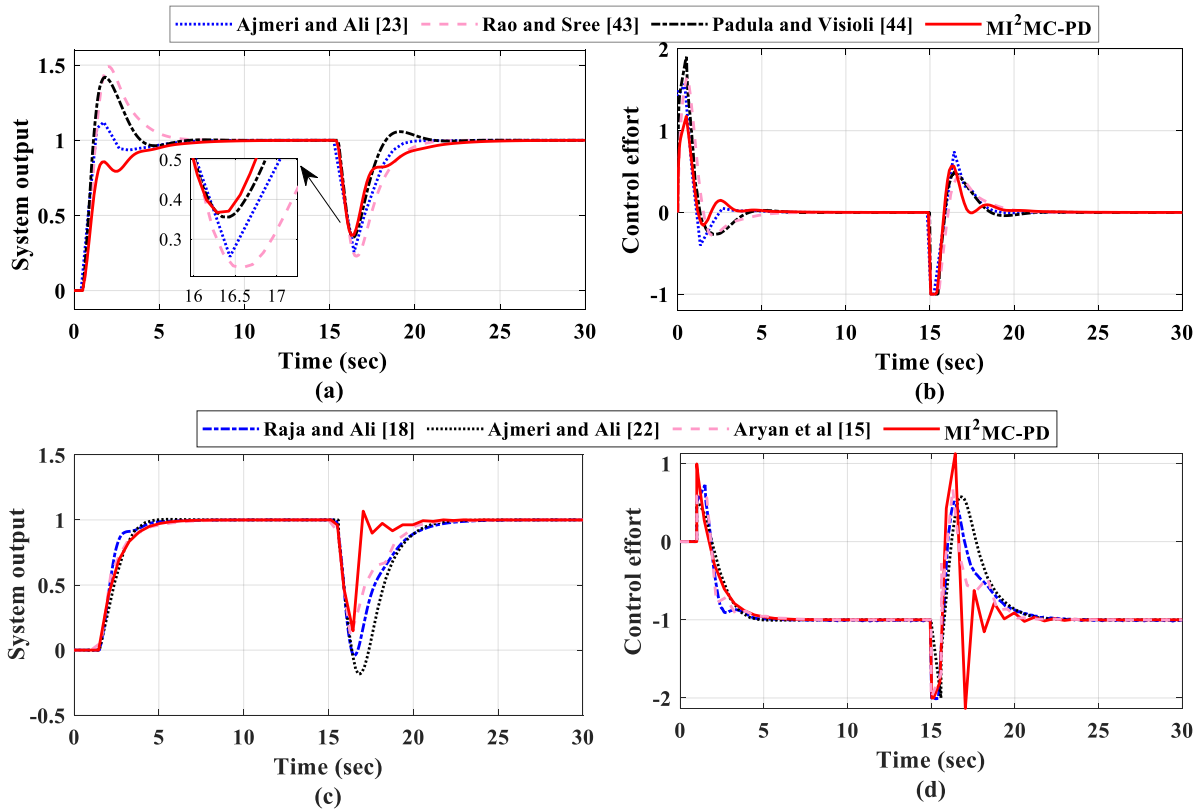

Figure 9. Plots for Example-1 (a) Dynamic output response for $G_p(s) = e^{-0.5s}/s$ (b) Control efforts for $G_p(s) = e^{-0.5s}/s$, Plots for Example-2 (c) Dynamic output response for $G_p(s) = e^{-0.5s}/(s-1)$ (d) Control efforts for $G_p(s) = e^{-0.5s}/(s-1)$

5.1.2 Example 2 (UFOPTD). The following UFOPTD process is considered:

$$G_P(s) = \frac{e^{-0.5s}}{s-1} \tag{28}$$

For the process given in (28), the PI-PD binal-loop structure was suggested by Raja and Ali [18] with controller settings K_p = 1.56, T_d = 0.250, K_c =1.186 and T_i =0.512. In Ajmeri and Ali [22], a B-DoF control scheme was utilized with settings K_{p2} = 1.790, T_{i2} =5, K_{p1} = 0.5, T_{i1} =0.25, K_c = 4, α=0.25 and β=0.098. Aryan et al. [15] reported a non-decoupled RIMC-PD binal-loop scheme with the following parameter values: K_C=1.8123, σ=0.0241 and λ=0.9176. The inner loop of Raja and Ali [18], Aryan et al. [15] and the outer-loop of Ajmeri and Ali [22] were designed for an M_S value of 2. To assess the regulatory behavior, D=-0.1 is applied at t=15 sec. The strategy suggested in this work delivers a comparable servo but enhanced regulatory response as evident from Figures 9(c) and 9(d). The PU_s post disturbance is significantly lesser than the other three methods as evident from Table 6. Due to this, the regulatory performance measures are also improved. The MI²MC-PD scheme's IAE of 2.450 for Y/D is remarkably less than Raja and Ali's [18] IAE of 3.622 and Ajmeri and Ali's [22] IAE of 4.304 (refer to Table 6). A similar trend is observed in the ISE measure as well. It is also worth mentioning that these improvements in the performance measures of the suggested scheme are achieved at a much lesser M_{S1}=1.279.

Table 5. Suggested controller settings

	K_C	τ_D	λ	ψ
Example-1	1.200	0.201	1.50	0.0377
Example-2	2.659	0.201	1.00	0.0100

Table 6. Performance measures comparison of the closed-loop responses (nominal) for Examples 1 and 2

	Method	**PO_s/PU_s**		**T_s (sec)**		**IAE**		**ISE**		**M_s**	
		Y/R	**Y/D**	**Y/R**	**Y/D**	**Y/R**	**Y/D**	**Y/R**	**Y/D**	**Outer**	**Inner**
Example-1	Ajmeri and Ali [23]	1.120	0.6216	5.677	20.539	2.353	31.24	1.301	32.99	2.000	-
	Rao and Sree [43]	1.491	0.7638	5.701	20.823	1.883	1.611	1.131	0.827	1.790	-
	Padula and Visioli [44]	1.420	0.6457	5.659	20.538	1.645	10.25	0.960	0.439	1.674	-
	Proposed	**1.000**	**0.6070**	6.695	23.404	**1.586**	**1.289**	**0.952**	**0.438**	**1.205**	**1.358**
Example-2	Raja and Ali [18]	1.001	1.0418	4.666	22.488	1.302	3.622	0.947	2.421	1.484	2.000
	Ajmeri and Ali [22]	1.005	1.2760	3.280	21.240	1.514	4.304	1.107	3.343	2.000	-
	Aryan et al. [15]	1.000	1.0230	5.594	21.031	1.464	3.286	1.107	3.343	1.500	2.000
	Proposed	**1.000**	**0.8232**	5.392	**20.127**	1.517	**2.450**	1.011	**1.476**	**1.279**	2.447

Table 7. ISE and IAE measures for different perturbation levels for Example-1

Perturbation	$G_{Po}(s)$	**Method**	**IAE**		**ISE**	
			Y/R	**Y/D**	**Y/R**	**Y/D**
10%	$\frac{1.1e^{-0.55s}}{s}$	Ajmeri and Ali [23]	1.341	31.240	0.8535	33.030
		Rao and Sree [43]	1.921	1.6100	1.2670	0.9051
		Padula and Visioli [44]	1.556	0.9838	1.0530	0.5039
		Proposed	1.586	1.2890	0.9866	**0.4964**
20%	$\frac{1.2e^{-0.6s}}{s}$	Ajmeri and Ali [23]	1.684	31.240	0.9932	33.160
		Rao and Sree [43]	2.212	1.6220	1.5360	1.0410
		Padula and Visioli [44]	1.825	1.1250	1.2830	0.8327
		Proposed	2.109	1.7800	**1.1300**	**0.7038**

Table 8. Higher-order processes with their reduced model for controller design

Example	**Process (For simulation)**	**Reduced model (For controller design)**	**Model reduction method**	**Reduced model category**
3	$\frac{e^{-0.5s}}{(5s-1)(0.5s+1)(2s+1)}$	$\frac{e^{-0.939s}}{(5s-1)(2.07s+1)}$	Dominant pole method (Tan et al. [45])	USOPTD
4	$\frac{e^{-5s}}{s(10s+1)(s+1)(0.5s+1)(0.25s+1)}$	$\frac{e^{-6.667s}}{s(10.141s+1)}$	Relay feedback identification (Kaya [46])	SOIPTD

5.3 Higher-order examples

To show the applicability of the suggested control scheme on higher-order processes, two such integrating and unstable examples are considered. Though the reduced model is utilized for controller design purposes, the higher-order process is simulated to investigate the effectiveness of the suggested control strategy (Refer to Table 8). Constrained K_C-τ_D search space for obtaining optimal equilibrium location is shown in Figure 10. The final optimal settings from EO are given in Table 9. Table 10 and Table 11 present the performance measure comparison under nominal and perturbed conditions respectively. Once again, the perturbation

of ±20% in parameters is considered for both the higher-order examples (as in the previous section).

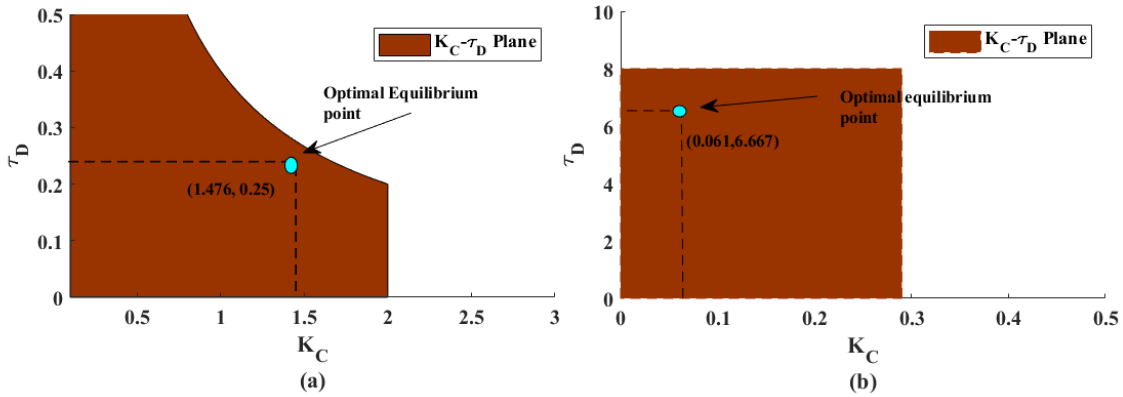

Figure 10. Constrained search-space with optimal equilibrium location (a) Example-5 (b) Example-6

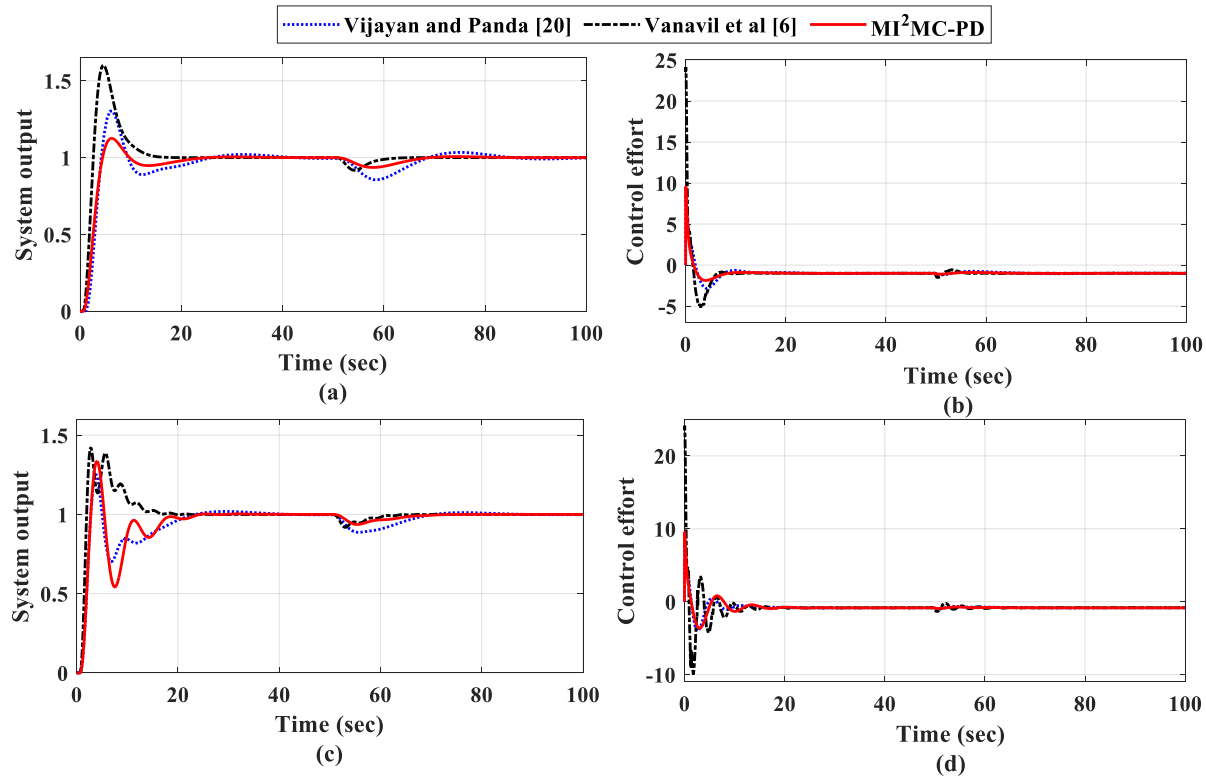

Figure 11. Plots for Example-3 (a) output response for $\frac{e^{-0.5s}}{(5s-1)(0.50s+1)(2s+1)}$ (b) control efforts for $\frac{e^{-0.5s}}{(5s-1)(0.50s+1)(2s+1)}$ (c) output response for $\frac{1.2e^{-0.6s}}{(4s-1)(0.40s+1)(1.6s+1)}$ d) control efforts for $\frac{1.2e^{-0.6s}}{(4s-1)(0.40s+1)(1.6s+1)}$

5.3.1 Example 3. A higher-order process with an unstable pole is given as

$$G_P(s) = \frac{e^{-0.5s}}{(5s-1)(0.5s+1)(2s+1)} \tag{29}$$

Using the reduced order model given in Table 11, the following PID-P binal-loop controller settings were obtained in Vijayan and Panda [20]: k_c = 0.5470, τ_I = 4.120, τ_D = 6.7344 and kc_1 = 1.3966 with λ= 0.60. Vanavil et al. [6] suggested the following PID controller with second order filter for the same reduced model as in Table 8:

$G_c = 7.0766\left(1+1/5.8911s+1.3603s\right)\left(0.0735s^2+0.4695s+1 \Big/ 0.0221s^2+0.1148s+1\right)$. For regulatory response analysis, D of value -0.1 is subjected at t=50 sec. Figures 11(a) and 11(b) present the nominal closed-loop response and the accordant control efforts while Figures 11(c) and 11(d) present the output responses and control efforts for the perturbed scenario. The PO_s achieved by Vijayan and Panda [20] and Vanavil et al. [6] are significantly higher than that of the MI^{2}MC-PD scheme for the servo response. Also, [20] has inferior disturbance rejection capability in comparison to the proposed scheme which is quite evident from Figures 11(a) and 11(b) and Table 10. The outer-loop M_S (M_{S1}=7.781) of Vijayan and Panda's [20] PID-P is much higher than that of MI^{2}MC-PD (M_{S1}=1.406). Hence the suggested controller is more robust than the PID-P scheme. This is exhibited in the former's improved performance measure under a perturbed scenario as presented in Table 11. The method reported in [6] does have satisfactory perturbed response but at a cost of significantly higher control efforts similar to the one witnessed in the nominal response making it inferior to the suggested scheme.

5.3.2 Example 4. A higher-order integrating plant model is given as

$$G_P(s) = \frac{e^{-5s}}{s(10s+1)(s+1)(0.5s+1)(0.25s+1)} \tag{30}$$

The I-PD binal-loop structure by Kaya and Peker [30] was designed for the approximated SOIPTD model as mentioned in Table 8 with the following settings: K_c = 0.170, T_i = 27.304, T_d = 7.2822. Alyoussef and Kaya [27] also designed their PI-PD scheme based on the same approximated SOITD model with settings K_f = 0.0943, K_d = 1.2701, K_P = 0.0713 and K_i = 0.0052. Moreover, Chakraborty et al. [29] controlled the process given in (31) by approximating it to an IPTD model ($0.561e^{-14.802s}/s$) to compute their I-PD controller settings (K_c = 0.102, T_i = 52.595 and T_d = 7.148). For regulatory response analysis, D is subjected -0.1 at t=250 sec. From Figures 12(a) and 12(b), which illustrate the nominal output response and control efforts, it can be understood that the I-PD scheme of Chakraborty et al. [29] is exhibiting inferior response with considerably large T_s for both servo as well as regulatory response and higher regulatory PU_s. Though Kaya and Peker [30] show slightly better T_s after disturbance rejection, the PU_s value is more than that of the proposed scheme. Figures 12(c) and 12(d) present the output responses and control efforts for the perturbed case. It is observed that both I-PD controller [30] and PI-PD of Alyoussef and Kaya [27] are unable to handle the perturbed plant with its original settings and give an oscillatory response. The suggested method has a significantly lesser ISE value for both nominal and perturbed scenarios than that of the two I-PD and PI-PD methods as evident from Table 10 and Table 11. The enhanced response of the suggested MI^{2}MC-PD is achieved at much lesser maximum sensitivities (M_{S1}=1.352, M_{S2}=1.450) than the other three discussed methods (refer to Table 10).

Table 9. Suggested controller settings

	K_C	τ_D	λ	ψ
Example-3	1.476	0.250	1.00	0.0102
Example-4	0.061	6.667	1.50	0.0108

Table 10. Performance measures comparison of the closed-loop responses (nominal) for Examples 3 and 4

	Method	PO_s/PU_s		T_s (sec)		IAE		ISE		M_s	
		Y/R	Y/D	Y/R	Y/D	Y/R	Y/D	Y/R	Y/D	Outer	Inner
Example-3	Vijayan and Panda [20]	1.303	0.1411	32.845	96.915	5.128	1.748	2.767	0.150	7.781	1.914
	Vanavil et al. [6]	1.601	0.0817	13.312	63.879	4.465	0.716	2.591	0.033	1.571	-
	Proposed	**1.125**	**0.0645**	20.058	83.182	**3.508**	**0.671**	**2.146**	**0.028**	**1.406**	3.957
Example-4	Kaya and Peker [30]	1.027	0.7400	52.833	351.21	28.46	516.1	23.32	541.3	1.317	2.886
	Chakraborty et al. [29]	1.001	1.0648	143.96	405.49	52.64	551.7	36.86	638.5	1.931	1.808
	Alyoussef and Kaya [27]	1.095	0.7440	79.470	331.05	21.37	19.65	16.43	9.815	3.370	-
	Proposed	1.037	**0.6733**	**72.047**	360.09	**13.70**	23.64	**9.042**	10.64	**1.352**	**1.450**

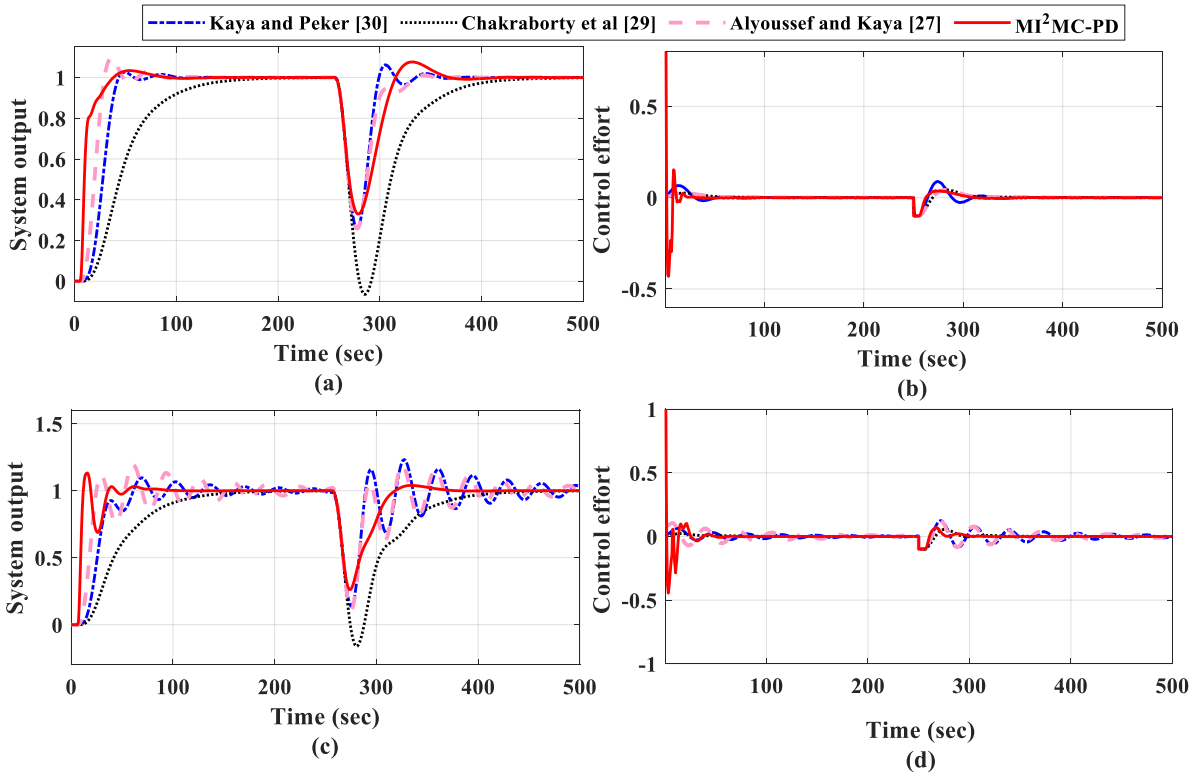

Figure 12. Plots for Example-4 (a) output response for $\frac{e^{-5s}}{s(10s+1)(s+1)(0.5s+1)(0.25s+1)}$ (b) control efforts for $\frac{e^{-5s}}{s(10s+1)(s+1)(0.5s+1)(0.25s+1)}$ (c) output response for $\frac{1.2e^{-6s}}{s(8s+1)(0.8s+1)(0.4s+1)(0.2s+1)}$ (d) control efforts for $\frac{1.2e^{-6s}}{s(8s+1)(0.8s+1)(0.4s+1)(0.2s+1)}$

Table 11. ISE and IAE measures for different perturbation levels for Examples 3 and 4

	Perturbation	$G_{Po}(s)$	Method	IAE		ISE	
				Y/R	Y/D	Y/R	Y/D
Example-3	10%	$\frac{1.1e^{-0.55s}}{(4.5s-1)(0.45s+1)(1.8s+1)}$	Vijayan and Panda [20]	4.570	1.66	2.110	0.1294
			Vanavil et al. [6]	4.219	0.717	2.273	0.0320
			Proposed	**3.920**	**0.633**	**2.052**	**0.0271**
	20%	$\frac{1.2e^{-0.6s}}{(4s-1)(0.4s+1)(1.6s+1)}$	Vijayan and Panda [20]	4.794	1.314	2.431	0.0989
			Vanavil et al. [6]	5.667	0.617	2.828	0.0299
			Proposed	**4.724**	**0.558**	**2.366**	**0.0219**
	30%		Vijayan and Panda [20]	10.20	1.232	2.912	0.0911

		$\frac{1.3e^{-0.65s}}{(3.5s-1)(0.35s+1)(1.4s+1)}$	Vanavil et al. [6]	-	-	-	-
			Proposed	**5.180**	**0.584**	**2.706**	**0.0212**
Example-4	10%	$\frac{1.1e^{-5.5s}}{s(9s+1)(0.9s+1)(0.45s+1)(0.225s+1)}$	Kaya and Peker [30]	29.07	516.1	22.64	541.8
			Chakraborty et al. [29]	52.61	551.7	36.12	638.2
			Alyoussef and Kaya [27]	22.92	21.21	16.03	10.08
			Proposed	**12.92**	**21.20**	**8.873**	**9.810**
	20%	$\frac{1.2e^{-6s}}{s(8s+1)(0.8s+1)(0.4s+1)(0.2s+1)}$	Kaya and Peker [30]	34.03	515.9	22.36	544.3
			Chakraborty et al. [29]	52.64	551.7	35.50	638.0
			Alyoussef and Kaya [27]	32.75	31.23	16.74	12.33
			Proposed	**14.27**	**21.32**	**9.476**	**10.07**
	30%	$\frac{1.3e^{-6.5s}}{s(7s+1)(0.7s+1)(0.35s+1)(0.175s+1)}$	Kaya and Peker [30]	29.07	516.1	22.64	541.8
			Chakraborty et al. [29]	52.61	551.7	36.12	638.2
			Alyoussef and Kaya [27]	22.93	21.05	16.01	10.07
			Proposed	24.04	**19.43**	**12.81**	**8.884**

5.4 Robust stability analysis

To evaluate the robustness of the MI^{2}MC-PD controller scheme against uncertainties in the estimated model ($G_{Po}(j\omega)$), an examination is conducted using the subsequent closed-loop robust stability condition [15]:

$$\|G_P(j\omega)H_{CS}(j\omega)\| < 1 \quad \forall\omega \in (-\infty, \infty) \tag{31}$$

where $U_N(j\omega)$ is the plant model's uncertainty norm and $H_{CS}(j\omega)$ is the closed-loop complementary sensitivity. $U_N(j\omega)$ is expressed as

$$U_N(j\omega) = \left|\frac{G_{Po}(j\omega) - G_P(j\omega)}{G_{Po}(j\omega)}\right| \tag{32}$$

Considering uncertainties of K , θ, $\tau_1$and τ_2 as $\Delta K, \Delta\theta, \Delta\tau_1$ and $\Delta\tau_2$ in (32), (31) becomes

$$\|H_{CS}(j\omega)\|_\infty < \left|\frac{\left(1-\frac{j\omega\Delta\tau_1}{j\omega\tau_1+1}\right)\left(1-\frac{j\omega\Delta\tau_2}{j\omega\tau_2+1}\right)}{\left(1+\frac{\Delta K}{K}\right)e^{-j\omega\Delta\theta} - \left(1-\frac{j\omega\Delta\tau_1}{j\omega\tau_1+1}\right)\left(1-\frac{j\omega\Delta\tau_2}{j\omega\tau_2+1}\right)}\right| \forall\omega > 0 \tag{33}$$

Figure 13 shows Bode magnitude charts (for $H_{CS}(j\omega)$ and $U_N(j\omega)$) for a 20% uncertainty. The complementary sensitivity for outer and inner-loops are calculated separately and denoted by H_{CS1} and H_{CS2} respectively. As can be seen, all of the cases fulfil the inequality relation of (33) and hence the requirement for robust stability of the binal-loops is satisfied.

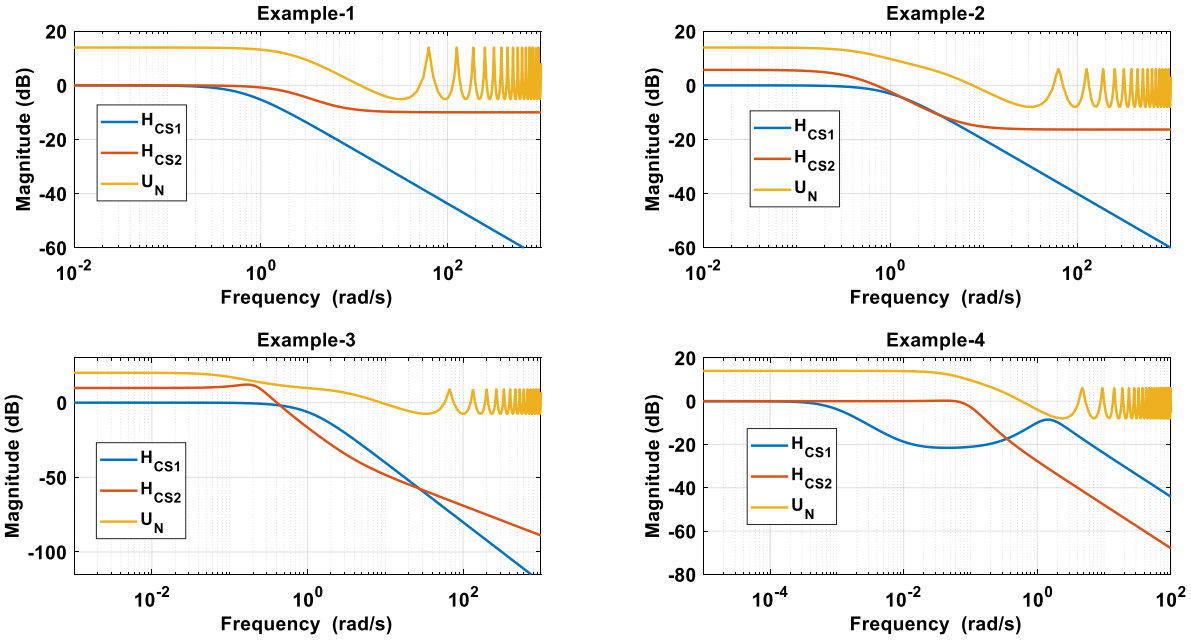

Figure 13. Magnitude plots of H_{CS1}, H_{CS2} and U_N for all examples

5.5 Pole-zero Plots

In this section, the stabilizing effect of the PD controller (designed in Section 3.2) is studied through pole-zero map (PZM). Figure 14 (a) presents the PZM of open-loop system, where the unstable poles are seen on the right-half of s-plane (corresponding to Examples 2 and 3). After stabilizing, the poles of the closed loop system are shifted to left half of s-plane (Figure 14 (b)). Similarly, the open-loop poles at the origin of s-plane (corresponding to Examples 1 and 4) are also shifted to the left half of the s-plane (Figure 14 (b)). Thus the unstable/integrating plants are stabilized by the action of PD controller as evident from Figure 14.

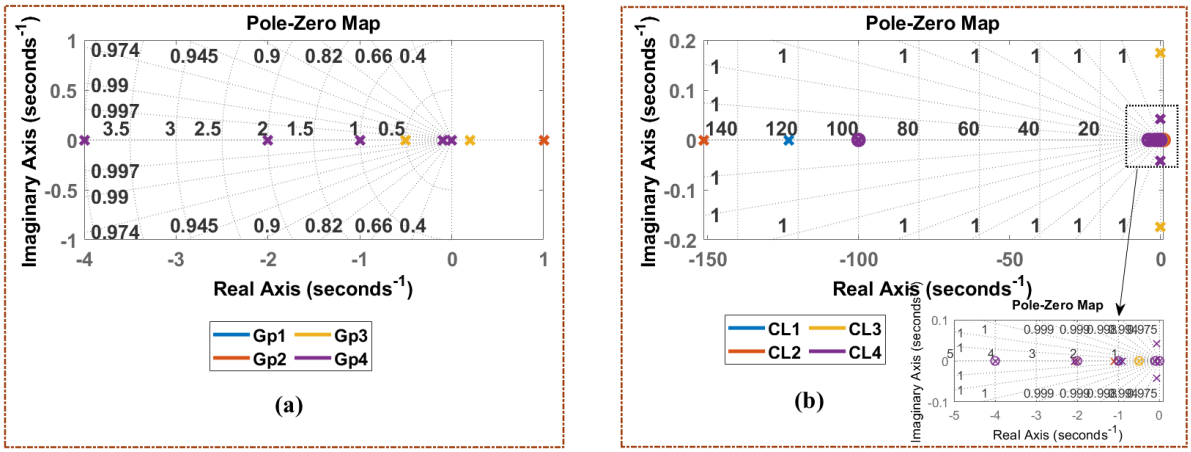

Figure 14. PZM (a) Open-loop plant (b) Stabilized closed-loop system

5.6 Effect of random noise and time-varying output disturbance signal

Noise can arise due to various reasons in a plant. Its source and nature are often unknown which makes the controller's job tough. Also, the disturbance entering the plant may not have a fixed value. A robust controller should be such that it minimizes the effect of such signals. The

process discussed in example-4 is subjected to a Gaussian noise (mean=0, variance=0.001) along with a time-varying output disturbance (refer to Figure 2) given by

$$G_{PD} = \frac{e^{-10s}}{s(s+1)} \tag{35}$$

Original controller settings (given in Table 9) have been retained while performing this simulation. The output response to unit step 'R' and time-varying G_{PD} along with control efforts are shown. It can be observed from Figure 15 that the suggested MI^{2}MC-PD controller performs satisfactorily amid the noise and time-varying disturbances.

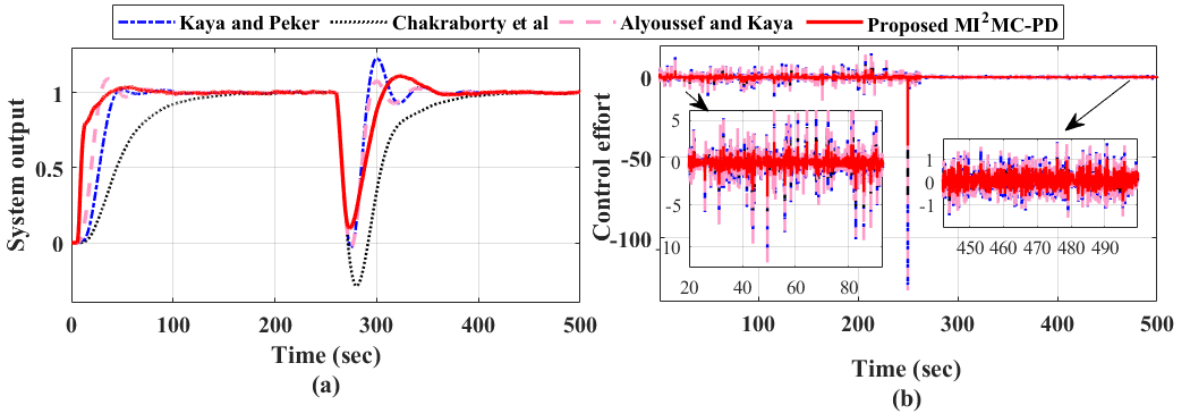

Figure 15. (a) Output response and (b) control efforts amid the noise and time-varying disturbance

5.7 Experimental verification using magnetic levitation (MAGLEV) setup

The effectiveness of the MI^{2}MC-PD approach is illustrated using a Feedback Instruments MAGLEV system (Model No. 33-210) (refer to Figure 16(a)). Hardware-in-loop (HIL) testing is used to run the simulation in real time. With this method, Simulink is used to simulate the controllers and frequency-shifted model shown in Figure 16(b). The hardware configuration, which is interfaced with a bi-directional 33-210 I/O card, then takes the position of the process transfer function, or 'G_P'. The MAGLEV arrangement is thus subjected to the control signals produced by the program. The metal ball's position is intended to be maintained at that location by the controller design. Figure 16(b) shows the schematic diagram for the MAGLEV configuration. The setup is identified as a UFOPTD process model [28, 47] with system identification toolbox at 97.8% model accuracy as

$$G_P(s) = \frac{-0.4502e^{-0.0201s}}{(-0.02234s+1)} \tag{36}$$

Following the design procedure, the MI^{2}MC-PD controllers and augmented model for this setup are found to be: $Gc_1(s) = (0.0388s-1)/1.1848(0.1276s+1)$, $Gc_2 = 2.6(1+0.01s)$ and $\hat{G}_P = 1.1848e^{-0.0201s}/(0.0388s-1)$. At t=0 sec, the metal ball is first positioned at a location that corresponds to R=15mV. The transient actions are not displayed because this procedure is done mechanically. At t=15 sec, the position is adjusted to R=55mV. To examine the servo behavior, three reference signal types—square, sinusoidal, and step—are taken into consideration. For the sinusoidal and square references, the amplitude and frequency are assumed to be 3.4 mV and 1 Hz, respectively. At t=20 sec, a disturbance of D=1 is introduced for the regulatory response. The ability of the MI^{2}MC-PD control strategy to make the metallic ball track the desired reference (of step, sinusoidal and square types) amid disturbance is

demonstrated in Figure 17. The control efforts do show some fluctuations, but it is well within the tolerance level of the actuator and hence feasible for the appended MAGLEV setup.

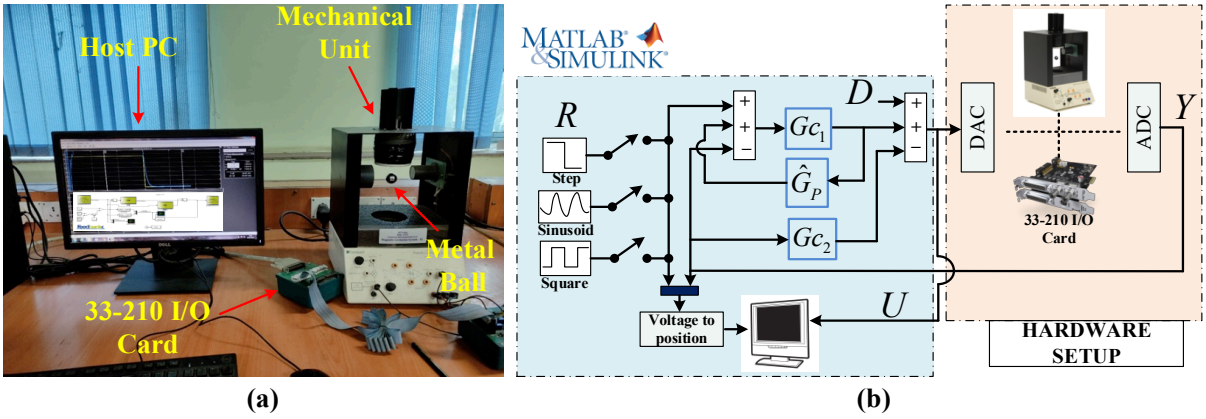

Figure 16. (a) MAGLEV experiment setup (b) Block diagram for implementing the suggested control scheme

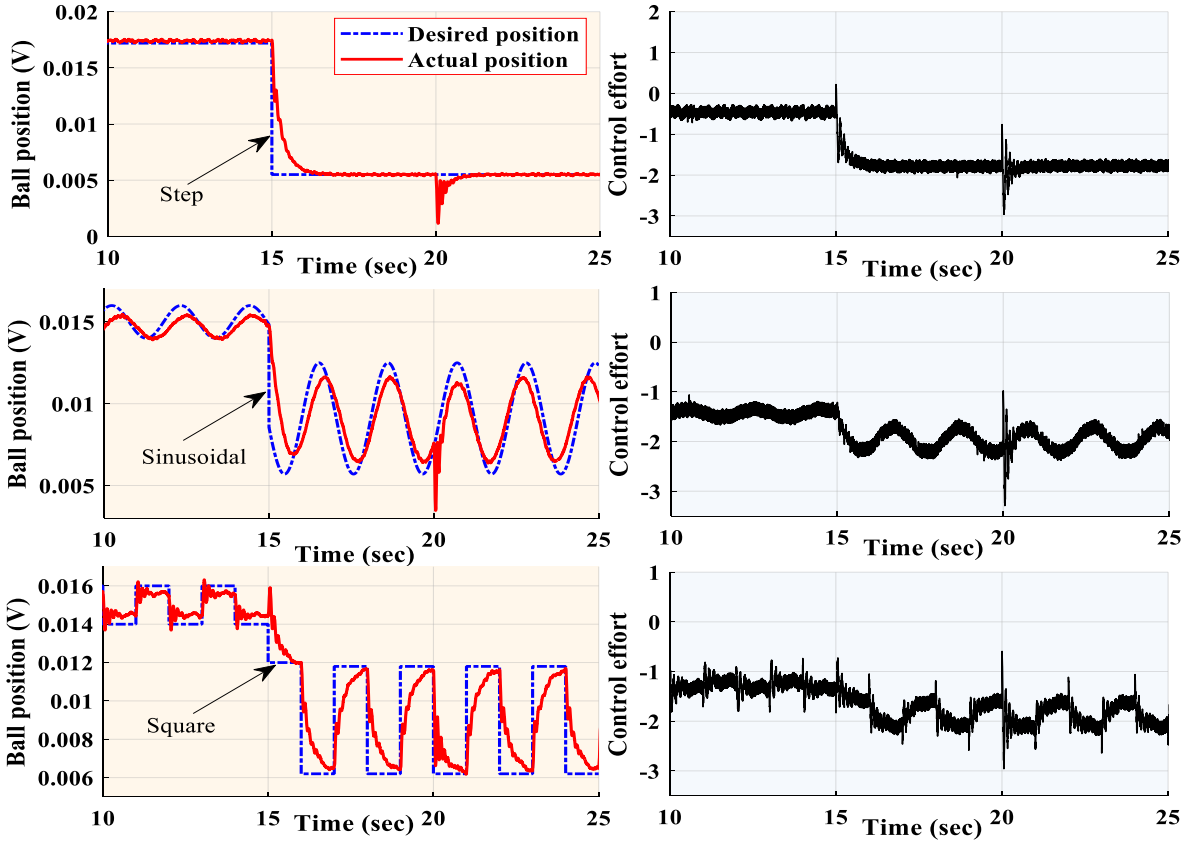

Figure 17. Output response and required control effort for the MAGLEV experiment

6 | CONCLUSION AND FUTURE SCOPE

This work explores the modification of an inferred internal model control-proportional derivative (MI^{2}MC-PD) decoupled binal-loop controller to be applied to a class of unstable and integrating industrial processes with dead-time. The inner-loop stabilization is achieved by the PD controller. The Routh-Hurwitz condition gives the constrained search space for PD settings which along with the outer-loop MI^{2}MC controller parameters are optimally tuned with a recent metaheuristic algorithm called equilibrium optimizer (EO). EO finds the optimal equilibrium location of the suggested controller's tunables in the constrained search space with the

objective of reducing integral squared error (ISE). The justification for the selection of ISE as the objective cost function is shown with simulations. The variation of robustness parameter ψ on the closed-loop behavior is studied in both time and frequency domains. The suggested method is applied to a variety of benchmark unstable and integrating processes for comparing reference following and disturbance rejection capabilities with existing methods. The comparison includes dynamic time-domain measures such as settling time, overshoot and undershoots along with the integral performance measures. The maximum sensitivity (M_S) values of outer and inner loops are calculated separately to vindicate the robustness of the MI^{2}MC-PD scheme. Particularly, for a third-order unstable process, the suggested method provided an improvement of 15.82% in the servo response and over 118% in the regulatory behavior at an M_S value of 1.406 as opposed to 7.781 of the compared literature. A similar trend can also be observed in other examples thereby indicating the superior performance-robustness tradeoff of the MI^{2}MC-PD design. It is also shown that the suggested method works considerably well for the process models having perturbation as high as 30% in its parameters exhibiting the scheme's robust operation. In the future, this work can be extended to control other classes of processes such as the double integral and non-minimum phase systems which would require a redesign of the inner-loop controller. The proposed control strategy can be further modified to handle other types of challenging time-varying disturbances such as ramp disturbances as a possible extension of the work.

Data availability statement:
The authors confirm that data and materials that support the results or analyses presented in this paper are freely available upon request.

Disclosure statement:
No potential conflict of interest was reported by the author(s).

Acknowledgement:

This work has received support from the Catalan Government under Project 2022 SGR 197 and by the Spanish Government under MICINN projects PID2019-105434RB-C33 and TED2021-806 129134B-I00 co-funded with the European Union ERDF funds.

References

[1] Kumari S, Aryan P, Kumar D and Raja GL (2022) Hybrid dual-loop control method for dead-time second-order unstable inverse response plants with a case study on CSTR. *International Journal of Chemical Reactor Engineering*.

[2] Seshagiri Rao A and Chidambaram M (2012) PI/PID controllers design for integrating and unstable systems. In *Advances in Industrial Control* (Issue 9781447124245).

[3] Shamsuzzoha, M., & Raja, G. L. (2023). Introductory chapter: PID-based industrial process control. In PID Control for Linear and Nonlinear Industrial Processes. IntechOpen.

[4] Sree RP and Chidambaram M (2003) Control of unstable bioreactor with dominant unstable zero. *Chemical and Biochemical Engineering Quarterly*, *17*(2), 139–145.

[5] Seshagiri Rao A, Rao VSR and Chidambaram M (2009) Direct synthesis-based controller design for integrating processes with time delay. *Journal of the Franklin Institute*, *346*(1), 38–56.

[6] Vanavil B, Chaitanya KK, and Rao AS (2015) Improved PID controller design for unstable time delay processes based on direct synthesis method and maximum sensitivity. *International Journal of Systems Science*, *46*(8), 1349–1366.

[7] Chanti Babu D, Santosh Kumar DB and Padma Sree R (2017) Tuning of PID Controllers for Unstable Systems Using Direct Synthesis Method. *Indian Chemical Engineer*, *59*(3), 215–241.

[8] Kumari S, Aryan P and Raja GL (2021) Design and simulation of a novel FOIMC-PD/P binal-loop control structure for CSTRs and bioreactors. *International Journal of Chemical Reactor Engineering*, *19*(12), 1287-1303.

[9] Ali A and Majhi S (2010) PID controller tuning for integrating processes. *ISA Transactions*, *49*(1), 70–78.

[10] Panda RC (2009) Synthesis of PID controller for unstable and integrating processes. *Chemical Engineering Science*, *64*(12), 2807–2816.

[11] Vanavil B, Anusha AVNL, Perumalsamy M and Rao AS (2014) Enhanced Imc-Pid Controller Design With Lead-Lag Filter for Unstable and Integrating Processes With Time Delay. *Chemical Engineering Communications*, *201*(11), 1468–1496.

[12] Verma B and Padhy PK (2019) Indirect IMC-PID controller design. *IET Control Theory and Applications*, *13*(2), 297–305.

[13] Arrieta O, Vilanova R and Visioli A (2011) Proportional-integral-derivative tuning for servo/regulation control operation for unstable and integrating processes. *Industrial and Engineering Chemistry Research*, *50*(6), 3327–3334.

[14] Ghousiya Begum K, Seshagiri Rao A and Radhakrishnan TK (2017) Enhanced IMC based PID controller design for non-minimum phase (NMP) integrating processes with time delays. *ISA Transactions*, *68*, 223–234.

[15] Aryan P, Raja GL and Vilanova R (2023a) Experimentally verified optimal bi-loop re-located IMC strategy for unstable and integrating systems with dead time. *International Journal of Systems Science*.

[16] Aryan P, Raja GL, Vilanova R and Meneses M (2023b) Repositioned Internal Model Control Strategy on Time-Delayed Industrial Processes With Inverse Behavior Using Equilibrium Optimizer. *IEEE Access*.

[17] Aryan P and Raja GL (2022) A novel equilibrium optimized binal-loop control scheme for unstable and integrating chemical processes involving dead time. *Int. J. Chem. React. Eng*, *1*, 20.

[18] Raja GL and Ali A (2021) New PI-PD Controller Design Strategy for Industrial Unstable and Integrating Processes with Dead Time and Inverse Response. *Journal of Control, Automation and Electrical Systems*, *32*(2), 266–280.

[19] Park JH, Sung SW and Lee IB (1998) An enhanced PID control strategy for unstable processes. *Automatica*, *34*(6), 751–756.

[20] Vijayan V and Panda RC (2012) Design of PID controllers in double feedback loops for SISO systems with set-point filters. *ISA Transactions*, *51*(4), 514–521.

[21] Cong ED, Hu MH, Tu ST, Xuan FZ and Shao HH (2014) A novel double loop control model design for chemical unstable processes. *ISA Transactions*, *53*(2), 497–507.

[22] Ajmeri M and Ali A (2015b) Two degree of freedom control scheme for unstable processes with small time delay. *ISA Transactions*, *56*, 308–326.

[23] Ajmeri M and Ali A (2015a) Direct synthesis based tuning of the parallel control structure for integrating processes. *International Journal of Systems Science*, *46*(13), 2461–2473.

[24] HongboZou and Li H (2015) Tuning of PI-PD controller using extended non-minimal state space model predictive control for the stabilized gasoline vapor pressure in a stabilized tower. *Chemometrics and Intelligent Laboratory Systems*, *142*, 1–8.

[25] Onat C (2019) A new design method for PI–PD control of unstable processes with dead time. *ISA Transactions*, *84*, 69–81.

[26] Alyoussef F and Kaya I (2022) Simple PI-PD tuning rules based on the centroid of the stability region for controlling unstable and integrating processes. *ISA transactions*.

[27] Alyoussef F and Kaya I (2023) Proportional–integral and proportional–derivative controller design based on analytically computed centroid point for controlling integrating processes. *Proceedings of the Institution of Mechanical Engineers, Part I: Journal of Systems and Control Engineering*, 09596518221143815.

[28] Irshad M and Ali A (2020) Robust PI-PD controller design for integrating and unstable processes. *IFAC-PapersOnLine*, *53*(1), 135–140.

[29] Chakraborty S, Ghosh S, and Naskar AK (2017) I-PD controller for integrating plus time-delay Processes. *IET Control Theory and Applications*, *11*(17), 3137–3145.

[30] Kaya I and Peker F (2020) Optimal I-PD controller design for setpoint tracking of integrating processes with time delay. *IET Control Theory and Applications*, *14*(18), 2814–2824.

[31] Kuehn DR and Porter J (1964) The application of linear programming techniques in process control. *IEEE Transactions on Applications and Industry*, *83*(75), 423-427.

[32] Richert D and Cortes J (2015) Robust distributed linear programming. *IEEE Transactions on Automatic Control*, *60*(10), 2567–2582.

[33] Faramarzi A, Heidarinejad M, Stephens B, and Mirjalili S (2020) Equilibrium optimizer: A novel optimization algorithm. *Knowledge-Based Systems*, *191*, 105190.

[34] Kaya I (2020) Integral-Proportional Derivative tuning for optimal closed loop responses to control integrating processes with inverse response. *Transactions of the Institute of Measurement and Control*, *42*(16), 3123–3134.

[35] Nema S and Kumar Padhy P (2015) Identification and cuckoo PI-PD controller design for stable and unstable processes. *Transactions of the Institute of Measurement and Control*, *37*(6), 708–720.

[36] Rai R and Dhal KG (2023). Recent Developments in Equilibrium Optimizer Algorithm: Its Variants and Applications. *Archives of Computational Methods in Engineering*, 1-54.

[37] Dogruer T (2023). Design of I-PD controller based modified smith predictor for processes with inverse response and time delay using equilibrium optimizer. *IEEE Access*, 11, 14636-14646.

[38] Kumar D, Aryan P and Raja GL (2022) Decoupled double-loop FOIMC-PD control architecture for double integral with dead time processes. *The Canadian Journal of Chemical Engineering*, *January*.

[39] Padhan DG and Majhi S (2012). Modified Smith predictor-based cascade control of unstable time delay processes. *ISA transactions*, *51*(1), 95-104.

[40] Vajta M (2000) Some remarks on Padé-approximations. In *Proceedings of the 3rd TEMPUS-INTCOM Symposium* (Vol. 242, pp. 1-6).

[41] Verma B and Padhy PK (2018). Optimal PID controller design with adjustable maximum sensitivity. *IET Control Theory & Applications*, 12(8), 1156-1165.

[42] Anand A, Aryan P, Kumari N and Raja GL (2022). Type-2 fuzzy-based branched controller tuned using arithmetic optimizer for load frequency control. *Energy Sources, Part A: Recovery, Utilization, and Environmental Effects*, *44*(2), 4575-4596.

[43] Nageswara Rao CV and Padma Sree R (2010). IMC Based Controller Design for Integrating Systems with Time Delay. *Indian Chemical Engineer*, *52*(3), 194–218.

[44] Padula F and Visioli A (2012). Optimal tuning rules for proportional-integral-derivative and fractional-order proportional-integral-derivative controllers for integral and unstable processes. *IET Control Theory & Applications*, *6*(6), 776-786.

[45] Tan W, Marquez HJ and Chen T (2003). IMC design for unstable processes with time delays. *Journal of process control*, *13*(3), 203-213.

[46] Kaya I (1999). *Relay feedback identification and model based controller design* (Doctoral dissertation, University of Sussex).

[47] Raja GL and Ali A. (2016). Modified parallel cascade control strategy for stable, unstable and integrating processes. Isa Transactions, 65, 394-406.